

**Structure and stability of  $\text{Al}_2\text{Fe}$  and  $\text{Al}_5\text{Fe}_2$ : First-principles total energy and phonon calculations**

M. Mihalkovič

*Institute of Physics, Slovak Academy of Sciences, SK-84228 Bratislava, Slovakia*

M. Widom

*Department of Physics, Carnegie Mellon University, Pittsburgh, Pennsylvania 15213, USA*

(Received 29 June 2011; revised manuscript received 11 November 2011; published 25 January 2012)

We employ first-principles total energy and phonon calculations to address the structure and stability of  $\text{Al}_2\text{Fe}$  and  $\text{Al}_5\text{Fe}_2$ . The observed structure of  $\text{Al}_2\text{Fe}$ , which is reported as stable in the assessed Al-Fe phase diagram, is distinguished by an unusually low triclinic symmetry. The initial crystallographic structure determination additionally featured an unusual hole large enough to accommodate an additional atom. Our calculations indicate that the hole must be filled, but predict that the triclinic structure is unstable relative to a simpler tetragonal structure based on the prototype  $\text{MoSi}_2$ . This tetragonal structure is interesting because it is predicted to be nonmagnetic, electrically insulating, and high density, while the triclinic structure is magnetic, metallic, and low density. We reconcile this seeming contradiction by demonstrating a high vibrational entropy that explains why the triclinic structure is stable at high temperatures. Finally, we note that orthorhombic  $\text{Al}_5\text{Fe}_2$  is also destabilized by the tetragonal structure but may be stabilized at high temperatures, again by vibrational entropy and partial occupancy associated with the diffusion of Al atoms along channels.

DOI: [10.1103/PhysRevB.85.014113](https://doi.org/10.1103/PhysRevB.85.014113)

PACS number(s): 61.66.-f, 63.20.dk, 64.30.-t, 71.20.Lp

**I. INTRODUCTION**

Aluminum-based intermetallic alloys with transition metals are of high interest for their complex crystalline and quasicrystalline structures, formed primarily with late transition metals, and their technologically useful compounds. Experimental phase diagram determination is difficult because many phases often exist within small composition ranges, many structures have unusually large unit cells, and many are intrinsically disordered, exhibiting mixed or partial site occupancy.

First-principles calculations can help resolve some uncertainties in the phase diagrams but are challenging themselves, for many of the same reasons. Intrinsic disorder requires studying alternative realizations of specific site occupancy. Some of the nearby competing phases may have unknown or poorly known structures. The large unit cells pose computational difficulties. Further complicating the study is the prevalence of magnetism among late transition metals.

The Al-Fe system is the prototype binary magnetic alloy based on a bcc structure.<sup>1</sup> The specific phase  $\text{Al}_5\text{Fe}_2$  is important as it forms at the junction layers of Fe with Zn during galvanizing treatments. Our own interest in the Al-Fe phase diagram derives from its complex and disordered crystal structures, some of which are related to quasicrystals.

The compound  $\text{Al}_2\text{Fe}$  is of special interest because of its unusual lowest-possible symmetry crystal structure, triclinic with space group 1 (P1) as determined by Corby and Black.<sup>2</sup> The initial crystallographic refinement, based on anomalous dispersion experiments, proposed an 18-atom unit cell (Pearson symbol aP18) with an unusual “hole” (see Fig. 1) that was sufficiently large to fit an entire Al or Fe atom. They also reported three sites of mixed occupancy,  $\text{Al}_{0.5}\text{Fe}_{0.5}$ .

Our preliminary first-principles calculations of total energy<sup>3</sup> showed that filling the hole was energetically favorable; thus we predicted the correct Pearson type as aP19.<sup>3</sup> However, we found this structure to be unstable with respect to competing phases, no matter how the hole was filled and how

the partial occupancy was resolved. A hypothetical tetragonal structure based on the  $\text{MoSi}_2$  prototype (Pearson symbol tI6) was predicted to be the true stable structure. This tI6 structure can be considered as an Al-rich variant of the B2 (Pearson cP2) structure of AlFe. It has never been observed experimentally, although it would be of high interest because it is predicted to be electrically insulating with a narrow gap.<sup>4,5</sup> Instead, multiple reexaminations confirm the stability of a triclinic structure for  $\text{Al}_2\text{Fe}$ . A recent crystallographic refinement,<sup>6</sup> utilizing conventional single-crystal diffraction, proposes that the space group is 2 (P $\bar{1}$ ) and fills the hole, confirming our predicted Pearson type aP19.

$\text{Al}_5\text{Fe}_2$  has an orthorhombic structure (Pearson type oC24; see Fig. 2) featuring a rigid framework of fully occupied Al and Fe sites as well as partially occupied Al sites confined within channels<sup>7</sup> that thread through the structure. Our optimal assignment of atoms to the partially occupied sites is predicted to be weakly unstable to decomposition into competing phases, including the hypothetical tetragonal structure.

Here we present a thorough study of the stability of  $\text{Al}_2\text{Fe}$  and  $\text{Al}_5\text{Fe}_2$  utilizing first-principles total energy calculations of low-temperature enthalpy supplemented by a phonon-based calculation of vibrational entropy yielding the high-temperature Gibbs free energy. Our calculations predict that the triclinic and orthorhombic structures are stabilized by vibrational entropy over the tetragonal structure at elevated temperatures. This occurs because aP19 has a much lower atomic density than tI6, and in oC24 the channel Al atoms are weakly bound and can actually diffuse at high temperature. A similar stabilization effect due to vibrational entropy was observed in the  $\theta/\theta'$  system of  $\text{Al}_2\text{Cu}$ .<sup>8</sup>

The remainder of this introduction surveys the global Al-Fe phase diagram and presents our calculational methods. We then present a thorough investigation of the energetics of plausible aP18 and aP19 structures, including the effects of magnetic moment formation and antiferromagnetism. Addressing  $\text{Al}_5\text{Fe}_2$ , we optimize the placement of Al atoms

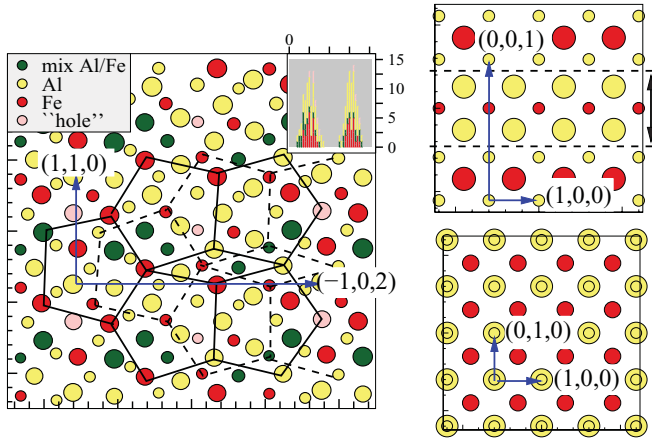


FIG. 1. (Color online) Left:  $\text{Al}_2\text{Fe}$  in the aP18 structure viewed along the pseudo-fivefold axis. Alternative pentagonal networks outlined in solid and dashed lines. Vertical positions are indicated by diameters. Inset shows histogram of positions in vertical direction, revealing layering at 2 Å spacing. Right: Two views of  $\text{Al}_2\text{Fe}$  in the hypothetical tI6 structure. Dashed lines in top figure define the slice shown in lower figure, chosen to highlight the B2 (CsCl) order.

among partially occupied channel sites. Finally we present vibrational densities of states that display large enhancements of low-frequency phonons in the aP19 and oC24 structures relative to tI6, explaining high-temperature stability.

### A. Assessed Al-Fe phase diagram

The Al-Fe phase diagram<sup>9</sup> contains at least six compounds as well as the two pure elements. Additionally there are at least three known metastable phases. Table I displays pertinent information including names, composition ranges, Pearson types, space groups, and assessed stability of all reported phases. Explicit coordinates and energies of all structures considered are posted in the “published” area of our alloy website.<sup>10</sup> Several of the phases report composition ranges associated with chemical substitution between Al and Fe

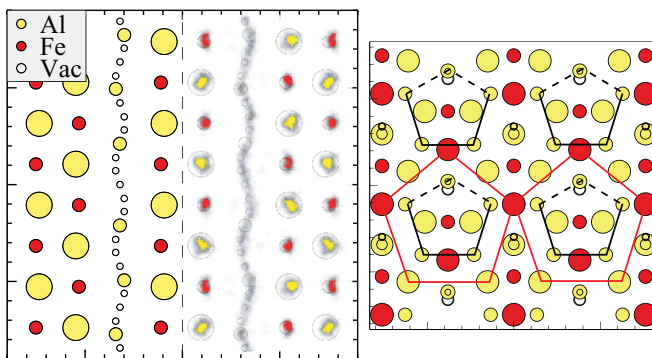


FIG. 2. (Color online) Left:  $\text{Al}_3\text{Fe}_2$  in the oC24 structure showing a  $1 \times 1 \times 3$  supercell with Al atoms placed among partially occupied sites to create oP44. Channel along  $c$  axis shows 4 occupied Al sites within the  $3c$  repeat. Right-hand side illustrates Al (yellow and gray) and Fe (red and gray) occupation as observed in first-principles molecular dynamics at  $T = 1300$  K. Right:  $\text{Al}_3\text{Fe}_2$  viewed along pseudo-fivefold axis. Alternative broken pentagonal motifs shown in solid and dashed lines.

TABLE I. Known phases of Al-Fe. Stability designation: S=stable to low  $T$ ; S?=stable at high temperature down to unknown  $T < 400$  °C; M=metastable; HT=stable at high temperature only. See Sec. IB for  $\Delta H_{\text{for}}$  and  $\Delta E$  (units are meV/atom). Average magnetic moment of Fe atoms  $\langle |m| \rangle$  (units are  $\mu_B/\text{Fe}$  atom).

Name	% Fe	Pearson	Group	Stab	$\Delta H_{\text{for}}$	$\Delta E$	$\langle  m  \rangle$
Al	0	cF4	$Fm\bar{3}m$	S	0	0	0
$\text{Al}_6\text{Fe}$	14	oC28	$Cmc2_1$	M	-205	5.8	0
$\text{Al}_9\text{Fe}_2$	18	mP22	$D8_d$	M	-258	9.5	0
$\text{Al}_3\text{Fe}$	23–26	mC102	$C2/m$	S	-347	0	0
$\text{Al}_5\text{Fe}_2$	27–30	oC24	$Cmcm$	S?	-349	1.5	0
$\text{Al}_2\text{Fe}$	33–34	aP18(19)	$P1(\bar{1})$	S?	-337	29.1	1.07
$\epsilon\text{-Al}_8\text{Fe}_5$	35–42	cI52	$I\bar{4}3m$	HT	-286	74.6	1.55
AlFe	45–77	cP2	$Pm\bar{3}m$	S	-346	0	0.68
$\text{AlFe}_2$	67	cF24	$Fd\bar{3}m$	M	-116	131.1	1.59
$\text{AlFe}_3$	66–77	cF16	$Fm\bar{3}m$	S	-198	0	1.96
Fe	55–100	cI2	$Im\bar{3}m$	S	0	0	2.18
Fe	98–100	cF4	$Fm\bar{3}m$	HT	+80	80.2	1.90

and also partial site occupancy. The  $\text{Al}_3\text{Fe}$  phase, more accurately described as  $\text{Al}_{13}\text{Fe}_4$ , is well known as a decagonal quasicrystal approximant. Structures of  $\text{Al}_2\text{Fe}$  and  $\text{Al}_5\text{Fe}_2$  also feature pentagonal networks.<sup>11</sup>

### B. Methods

Our calculations follow methods outlined in a prior paper.<sup>12</sup> We utilize VASP<sup>13,14</sup> to carry out first-principles total energy calculations in the PW91 generalized gradient approximation. Comparisons with the LDA and PBE density functionals confirm the principal findings based on PW91. We relax all atomic positions and lattice parameters, and increase our  $k$ -point densities until energies have converged. We adopt projector augmented wave potentials<sup>15,16</sup> and maintain a fixed energy cutoff of 267.9 eV (the default for Fe). All calculations considered the possibility of spin polarization, and utilize a medium precision setting which allows small wrap-around errors in Fourier transforms.

Given total energies for a variety of structures, we calculate the enthalpy of formation  $\Delta H_{\text{for}}$  which is the enthalpy of the structure relative to a tie line connecting the ground-state configurations of the pure elements. Formally, for a compound of stoichiometry  $\text{Al}_m\text{Fe}_n$  we define the composition variable  $x_{\text{Fe}} = n/(m+n)$  and the formation enthalpy

$$\Delta H_{\text{for}} = H(\text{Al}_m\text{Fe}_n) - [xH(\text{Fe}) + (1-x)H(\text{Al})], \quad (1)$$

where all enthalpies are per atom. Vertices of the convex hull of  $\Delta H(x_{\text{Fe}})$  constitute the predicted low-temperature stable structures. For structures that lie above the convex hull we calculate the instability energy  $\Delta E$  as the enthalpy difference relative to the convex hull at the same composition. When presented with multiple structure possibilities or mixed site occupancy, we examine all plausible structures and report the most energetically favorable.

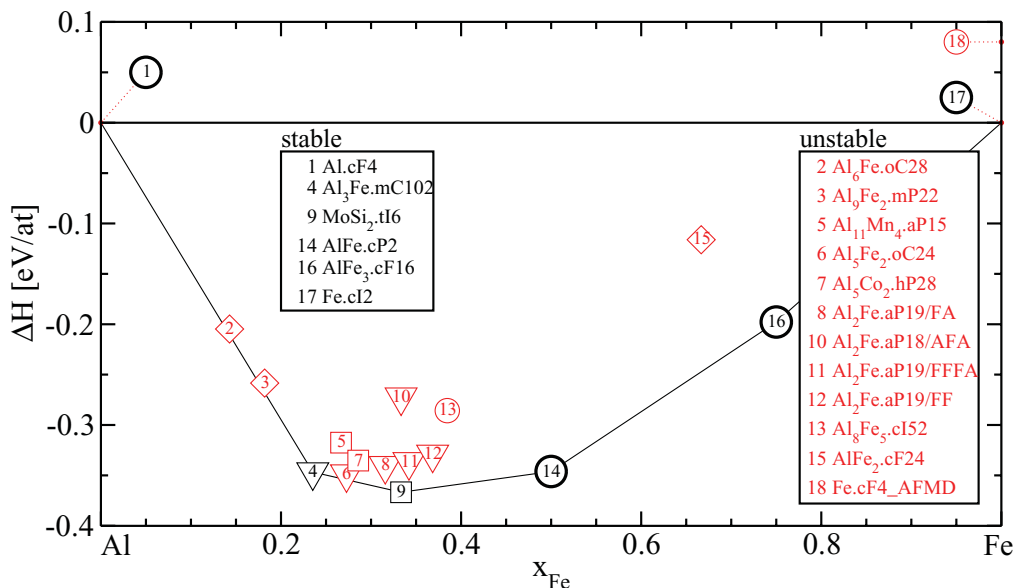


FIG. 3. (Color online) Enthalpies of formation of Al-Fe compounds. Plotting symbols: heavy circle=known stable; light circle=known high temperature; diamond=known metastable; triangle=unknown stability; square=unknown phase. Plotting colors: black=on convex hull; red=above convex hull. Notation A and F indicate Al or Fe on Wyckoff 1a positions M1, M2, and M3 (aP18) or Wyckoff 2i position Fe4 (aP19).

## II. RESULTS

### A. Global phase diagram

As illustrated in Fig. 3 our calculated enthalpies agree in almost every respect with the assessed phase diagram. All the phases that are known to be stable at low temperature (heavy circles) indeed reach the convex hull. Those known to be metastable (diamonds) or stable only at high temperatures (light circles) lie slightly above the convex hull. Of those whose low-temperature stability is uncertain (triangles), Al<sub>3</sub>Fe lies on the convex hull, while Al<sub>5</sub>Fe<sub>2</sub> and Al<sub>2</sub>Fe (aP18 and aP19) both lie slightly above.

The only serious discrepancy between the experimental phase diagram and our calculation is the presence of Al<sub>2</sub>Fe in the tI6 (prototype MoSi<sub>2</sub>) structure on the convex hull. This structure can be considered as a B2 (CsCl) structure with periodic stacking faults reversing the chemical order.

Its electronic density of states (see Fig. 4) exhibits a narrow gap.

Magnetism was found to be favorable in all the structures reported in Table I containing more than 33% Fe. Elemental Fe exhibits ferromagnetism in its low-temperature cI2 structure and modulated antiferromagnetism in its high-temperature cF4 structure. Al<sub>2</sub>Fe also exhibits long-wavelength antiferromagnetism in its aP18 and aP19 structures.

Our calculated total energies correctly predict the Al<sub>9</sub>Fe<sub>2</sub> and Al<sub>6</sub>Fe structures to be metastable in the Al-Fe alloy system, while the same structures are correctly predicted to be stable in the Al-Co and Al-Mn alloy systems, respectively.<sup>3,17</sup> Similarly, we correctly predict Al-Fe to be unstable when placed in the Al<sub>11</sub>Mn<sub>4</sub>.aP15 and Al<sub>5</sub>Co<sub>2</sub>.hP24 structures. Conversely, we correctly predict AlFe<sub>3</sub> stable in Al-Fe but unstable in both Al-Co and Al-Mn. This sensitivity to the small differences in interatomic bonding between Fe and its neighbors in the

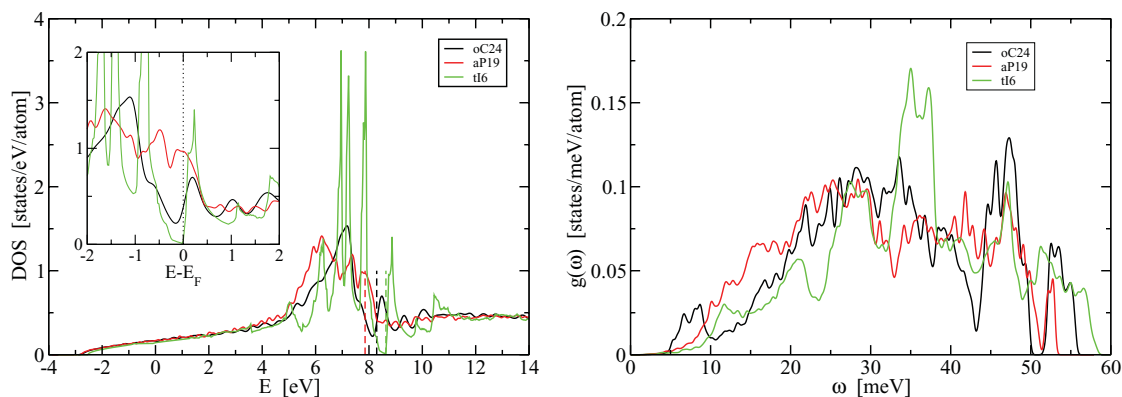


FIG. 4. (Color online) Left: Electronic densities of states of oC24 (oP44 variant), aP19 (FFFA variant), and tI6. For convenience the electronic DOS of aP19 is shown *without* spin polarization. Vertical dashed lines indicate Fermi energy. The gap in tI6 is predicted to be 0.11 eV. Right: Vibrational densities of states of oC24 (oP44 variant), aP19 (FFFA variant), and tI6.

periodic table, Co and Mn, gives us confidence in the validity of our first-principles total energies.

### B. $\text{Al}_2\text{Fe.aP18/aP19}$

The Corby and Black<sup>2</sup> structure with Pearson type aP18 possesses an unusually large hole. In addition three sites, labeled M1, M2, and M3, exhibit mixed  $\text{Al}_{0.5}\text{Fe}_{0.5}$  occupancy (marked in green in Fig. 1). We tested all eight arrangements of Al and Fe among these three sites (labeled AAA, AAF, . . . , FFF) within a single unit cell and found that none of them resulted in a stable structure. Additionally, all suffered rather large maximum atomic displacements of 0.3–0.4 Å. All structures except AAA favored weak ferromagnetism. Our optimal stoichiometric structure, AFA, exhibited magnetic moments averaging  $1 \mu_B/\text{Fe}$  atom, resulting in an energy drop of 26 meV/atom.

Previously,<sup>3</sup> we found that filling the Corby-Black hole with an Fe atom is energetically favorable, suggesting that aP19 is the correct Pearson type for this compound. The nominal composition  $\text{Al}_2\text{Fe}$  cannot be achieved in a single unit cell. Additionally, in the new structure refinement<sup>6</sup> there is a single site (Fe4, Wyckoff position 2i) with mixed  $\text{Al}_{0.295}\text{Fe}_{0.705}$  occupancy. For this reason we examine both Al and Fe on the Fe4 sites within a single unit cell (three possibilities labeled AA, AF=FA, FF), and we also examine a supercell doubled along the  $a$  axis with one of the four Fe4 sites replaced by Al (labeled FFFA).

In our single-cell aP19/FF ferromagnetic structure we find moments of  $1.1 \mu_B$  on Fe1,  $0.9$  on Fe2 sites,  $0.8$  on Fe3, and  $1.8$  on Fe4. In the supercell we find that long-period antiferromagnetism is favored over ferromagnetism by 3 meV/atom, consistent with the findings of incommensurate antiferromagnetism.<sup>18</sup> Magnetic moments in our aP19/FFFA antiferromagnetic structure were qualitatively similar in magnitude to our aP19/FF ferromagnetic structure except in the vicinity of Al substitutions on the Fe4 site. See our website<sup>10</sup> for further details. The electronic density of states of this structure (*without* magnetism) shows that the Fermi level lies in a peak of the density of states (see Fig. 4), consistent with the Stoner mechanism for ferromagnetism. Attempts to find disordered magnetic ground states by starting from randomly selected initial Fe moments of  $\pm 2 \mu_B$  did not succeed in lowering the total energy, suggesting a possible absence of spin glass order.<sup>19</sup> Likewise, runs utilizing noncollinear magnetism failed to reduce the energy.

In Fig. 3 we note a slope in the enthalpies of aP19 with respect to  $x_{\text{Fe}}$  so that  $\Delta E$  drops to as low as 9 meV/atom in the Al-rich limit of aP19/AA (not shown) at  $x_{\text{Fe}} = 0.263$ , while it rises to 33.3 meV/atom in the Fe-rich limit of aP19/FF (reference number 12 in Fig. 3) at  $x_{\text{Fe}} = 0.368$ . The optimal structure we found at the precise  $x_{\text{Fe}} = 0.333$  stoichiometry of  $\text{Al}_2\text{Fe}$  is a sixfold supercell of aP19 (not shown) containing 114 atoms and remaining unstable by 29 meV/atom. The experimentally reported composition is  $x_{\text{Fe}} = 0.337$ .

### C. $\text{Al}_5\text{Fe}_2$

The other phase of problematic stability is  $\text{Al}_5\text{Fe}_2$  (see Fig. 2). As noted previously this structure features pentagonal

networks as well as partially occupied “aluminum channels.” There are two such channels per unit cell, running parallel to the  $c$  axis. The density of the channels (i.e., the number of aluminums per  $c$  repeat per channel) can vary over a range of up to 1.5 Al/repeat/channel while maintaining favorable separations of 2.8 Å or greater. The partially occupied sites come in two types:<sup>20</sup> Wyckoff class 4b placed symmetrically between pairs of Fe atoms (refined occupancy 0.32), and Wyckoff class 8f displaced 0.75 Å away from 4b sites (refined occupancy 0.24).

After exploring many arrangements of Al atoms among the partially occupied sites, we find the energetically optimal structure occurs with four Al atoms in three repeats for a channel density of 4/3. We place two atoms on sites of class 4b, and two on sites of class 8f. The selection of sites is staggered in adjacent channels, resulting in a primitive orthorhombic structure (Pearson type oP44) for our optimized structure, while random placement of Al atoms among sites (e.g., at high temperature) restores the nominal oC24 unit cell.

The electronic density of states features a weak pseudogap (see Fig. 4), but the Fermi energy lies to the right-hand side, suggesting the pseudogap does not play an essential role in stabilization. An alternate structure placing five Al in four repeats produced a strong pseudogap with the Fermi energy at the minimum, but increased the energy by 4 meV/atom. Another alternate structure, placing an Fe atom in place of one of the channel Al atoms, increases the energy by 18 meV/atom, while creating a magnetic moment on the channel Fe atom<sup>21</sup> of  $2.2 \mu_B$ .

Our optimal structure would sit on the convex hull of enthalpy if it were not for the presence of the tI6 structure. Instead, it sits 1.5 meV/atom above the tie line joining  $\text{Al}_3\text{Fe}$  (mC102) to  $\text{Al}_2\text{Fe}$  (tI6), indicating that at low temperatures it will decompose into these structures.

## III. VIBRATIONAL AND CONFIGURATIONAL FREE ENERGIES

Despite extensive effort, we were unable to find enthalpy-minimizing structures for  $\text{Al}_2\text{Fe}$  or for  $\text{Al}_5\text{Fe}_2$ . All structures considered remained above the convex hull, as illustrated in Fig 3. Given that the assessed phase diagram does not assert low-temperature stability, we now consider the possibility that this structure is stabilized at high temperature by entropy. An entropy  $s$  per atom results in a free-energy reduction of  $Ts$  at temperature  $T$ . The obvious source of entropy is vibrational, arising from the low atomic density of aP19 and the Al channels of oC24.

The vibrational free energy can be obtained within the harmonic approximation by means of the quantum mechanical theory of phonons. For each phonon mode of vibrational frequency  $\omega$ , the temperature-dependent vibrational free energy (including zero-point energy, internal energy, and entropy) is  $\ln [2 \sinh(\hbar\omega/2k_B T)]$ . We then integrate this quantity over frequency, weighted by the vibrational density of states  $g(\omega)$  to obtain the full vibrational free energy

$$f_{\text{vib}}(T) = k_B T \int g(\omega) \ln [2 \sinh(\hbar\omega/2k_B T)] d\omega. \quad (2)$$

To calculate  $g(\omega)$  we employed the force constant method for phonon calculations,<sup>22</sup> in which we take a supercell of minimum edge length 8 Å and evaluate the second derivatives of total energy  $\partial^2 U / \partial \mathbf{R}_i \partial \mathbf{R}_j$  for all pairs of atoms  $i$  and  $j$ . The calculations utilized density functional perturbation theory as implemented in VASP, and employ an accurate precision that avoids Fourier transform wrap-around errors. We then construct the dynamical matrix<sup>23</sup>  $\mathbf{D}(\mathbf{k})$  on a dense mesh of  $k$ -points and evaluate the phonon frequencies. The resulting calculated vibrational densities of states are presented in Fig. 4.

Even with the hole filled, the atomic volume of Al<sub>2</sub>Fe in the aP19/FFFA structure is 13.48 Å<sup>3</sup>/atom while the atomic volume of tI6 is only 12.7 Å<sup>3</sup>/atom. The higher atomic volume of aP19 implies weaker bonding, consistent with lower enthalpy of formation. Weaker bonding suggests an enhanced density of low-frequency phonons that can increase vibrational entropy and correspondingly lower the vibrational free energy. Because Al<sub>2</sub>Fe.aP19/FFFA is at very nearly the identical composition to Al<sub>2</sub>Fe.tI6, we need only compare the vibrational free energies of these two structures (in principle we should include a small admixture of AlFe.cI2, but with *very* low weighting). The excess density of low-frequency phonons is clearly evident over the frequency range 10–30 meV and yields a reduction in free energy of 38 meV/atom by the time we reach  $T = 1000$  K. Comparing the free energies of tI6 and oP19, we find that aP19 is stabilized over tI6 for temperatures greater than 380 K.

For Al<sub>5</sub>Fe<sub>2</sub> in the optimal oP44 structure, we see an excess density of low-frequency phonons in the range 5–10 meV that leads to a free-energy reduction of 20 meV/atom by the time we reach  $T = 1000$  K. These phonon modes are localized in the channel Al atoms and are primarily polarized along the  $c$  axis. That is, they correspond to oscillations along the channels. These low-frequency modes are able to create an appreciable excess entropy at temperatures as low as 30 K.<sup>21</sup> Comparing the free energies with the weighted average of mC102 and tI6, we find that oC24 is stabilized for temperatures greater than 320 K.

Full anharmonic vibrational free energy calculations should be performed for Al<sub>5</sub>Fe<sub>2</sub>, owing to the liquid-like motion of the channel Al atoms. This behavior is evident in Fig. 2 where we present the occupation densities collected using VASP molecular dynamics. This run was carried out within the oP44 cell for a duration of 15 ps at temperature  $T = 1300$  K. During the simulation the channel Al atoms diffused in a liquid-like manner along the channels. By sampling the entire set of channel Al sites, the symmetry rises from oP44 to oC24, and the original unit cell is restored. Clearly the associated entropy is poorly represented using the harmonic approximation based on low-frequency phonons.

#### IV. CONCLUSION

This paper addresses the stability of two phases Al<sub>2</sub>Fe (aP18/19) and Al<sub>5</sub>Fe<sub>2</sub> (oC24) that are experimentally observed in the Al-Fe phase diagram. These phases are predicted as unstable according to first-principles calculations, which instead predict stability of a hypothetical (and so far never observed) structure based on the prototype MoSi<sub>2</sub> (tI6). We show that each of the observed phases may be stabilized over the hypothetical one at high temperatures by their vibrational entropy. The high vibrational entropy arises from anomalously low atomic density in the case of aP19, and from diffusion of Al atoms within channels in the case of oC24. Presumably the high-temperature stability of the observed phases inhibits formation of the low-temperature tI6 phase because atomic diffusion is slow at the low temperatures at which it is stable. It would be very interesting if this predicted low-temperature phase can be formed, because it is expected to be a semiconducting compound formed from good metals.

#### ACKNOWLEDGMENTS

This work was supported in part by Grants No. VEGA j2/0111/11 and No. APVV-0647-10.

<sup>1</sup>D. A. Contreras-Solorio, F. Mejia-Lira, J. L. Moran-Lopez, and J. M. Sanchez, *Phys. Rev. B* **38**, 11481 (1988).

<sup>2</sup>R. N. Corby and P. J. Black, *Acta Crystallogr. B* **29**, 2669 (1973).

<sup>3</sup>M. Mihalkovič and M. Widom, Alloy Database [<http://alloy.phys.cmu.edu>].

<sup>4</sup>M. Weinert and R. E. Watson, *Phys. Rev. B* **58**, 9732 (1998).

<sup>5</sup>M. Krajci and J. Hafner, *J. Phys. Condens. Matter* **14**, 5755 (2002).

<sup>6</sup>I. Chumak, K. W. Richter, and H. Ehrenberg, *Acta Crystallogr. C* **66**, i87 (2010).

<sup>7</sup>N. Gu, C. L. Henley, and M. Mihalkovič, *Philos. Mag.* **86**, 593 (2006).

<sup>8</sup>C. Wolverton and V. Ozolins, *Phys. Rev. Lett.* **86**, 5518 (2001).

<sup>9</sup>B. Sundman, I. Ohnuma, N. Dupin, U. R. Kattner, and S. G. Fries, *Acta Mater.* **57**, 2896 (2009).

<sup>10</sup>M. Mihalkovič and M. Widom, Alloy Database [<http://alloy.phys.cmu.edu/published/AlFe>].

<sup>11</sup>A. Hirata, Y. Mori, M. Ishimaru, and Y. Koyama, *Philos. Mag. Lett.* **88**, 491 (2008).

<sup>12</sup>M. Mihalkovič and M. Widom, *Phys. Rev. B* **70**, 144107 (2004).

<sup>13</sup>G. Kresse and J. Hafner, *Phys. Rev. B* **47**, 558 (1993).

<sup>14</sup>G. Kresse and J. Furthmuller, *Phys. Rev. B* **54**, 11169 (1996).

<sup>15</sup>P. E. Blochl, *Phys. Rev. B* **50**, 17953 (1994).

<sup>16</sup>G. Kresse and D. Joubert, *Phys. Rev. B* **59**, 1758 (1999).

<sup>17</sup>M. Mihalkovič and M. Widom, *Phys. Rev. B* **75**, 014207 (2007).

<sup>18</sup>D. Kaptás, E. Sváb, Z. Somogyvári, G. André, L. F. Kiss, J. Balogh, L. Bujdosó, T. Kemény, and I. Vincze, *Phys. Rev. B* **73**, 012401 (2006).

<sup>19</sup>C. S. Lue, Y. Öner, D. G. Naugle, and J. H. Ross, *Phys. Rev. B* **63**, 184405 (2001).

<sup>20</sup>U. Burkhardt, Y. Grin, M. Ellner, and K. Peters, *Acta Crystallogr. B* **50**, 313 (1994).

<sup>21</sup>J. Chi, X. Zheng, S. Y. Rodriguez, Y. Li, W. Guo, V. Gorunganti, K. D. D. Rathnayaka, and J. H. Ross, *Phys. Rev. B* **82**, 174419 (2010).

<sup>22</sup>G. Kresse, J. Furthmuller, and J. Hafner, *Europhys. Lett.* **32**, 729 (1995).

<sup>23</sup>N. W. Ashcroft and N. D. Mermin, *Solid State Physics* (Saunders, 1976).